AFRL-SR-AR-TR-10-0007

# REPORT DOCUMENTATION PAGE



**PLEASE DO NOT RETURN YOUR FORM TO THE ABOVE ADDRESS.**

| 1. REPORT DATE *(DD-MM-YYYY)* | 2. REPORT TYPE | 3. DATES COVERED *(From - To)* |
|---|---|---|
| 2009-02-28 | Final | 08/01/07 - 11/30/08 |

**4. TITLE AND SUBTITLE**
THZ-OSCILLATIONS IN GAN/ALUMINUM GAN SUPERLATTICES

**5a. CONTRACT NUMBER**

**5b. GRANT NUMBER**
FA9550-07-1-0525

**5c. PROGRAM ELEMENT NUMBER**

**6. AUTHOR(S)**
Hadis Morkoc, Ph.D.

**5d. PROJECT NUMBER**

**5e. TASK NUMBER**

**5f. WORK UNIT NUMBER**

**7. PERFORMING ORGANIZATION NAME(S) AND ADDRESS(ES)**
Virginia Commonwealth University
School of Engineering
Box 843068
Richmond, VA 23284-3068

**8. PERFORMING ORGANIZATION REPORT NUMBER**
Final Technical; Index 542109

**9. SPONSORING/MONITORING AGENCY NAME(S) AND ADDRESS(ES)**
AFOSR
875 N Randolph St, Rm. 3112
Arlington, VA 22203

**10. SPONSOR/MONITOR'S ACRONYM(S)**

**11. SPONSOR/MONITOR'S REPORT NUMBER(S)**

**12. DISTRIBUTION/AVAILABILITY STATEMENT**
Approved for Public Release; distribution is unlimited



**13. SUPPLEMENTARY NOTES**

**14. ABSTRACT**

**15. SUBJECT TERMS**

| 16. SECURITY CLASSIFICATION OF: | | | 17. LIMITATION OF ABSTRACT | 18. NUMBER OF PAGES | 19a. NAME OF RESPONSIBLE PERSON |
|---|---|---|---|---|---|
| a. REPORT | b. ABSTRACT | c. THIS PAGE | | | Hadis Morkoc |
| Unclassified | Unclassifed | Unclassified | SAR | | 19b. TELEPHONE NUMBER *(Include area code)* 804-827-3765 |

# Final Report

**Grant no:** FA9550-07-1-0525

**Report for period:** 08/2007 – 11/2008

**Principal Investigator:** Hadis Morkoç, hmorkoc@vcu.edu

**Organization:** Virginia Commonwealth University

**Title:** Terahertz generation in GaN/AlGaN superlattices

**Program manager:** Dr. Gernot S. Pomrenke
Optoelectronics and Nanotechnology
AFOSR/NE
Directorate of Physics and Electronics
Air Force Office of Scientific Research
875 North Randolph Street
Suite 325, Room 3112
Arlington, Virginia 22203-1768 USA
e-mail: gernot.pomrenke@afosr.af.mil
Tel: 703-696-8426
Fax: 703-696-8481

**Table of Contents**

## 1. Summary

Nitride semiconductors based heterostructures have so far been exploited for electronic devices utilizing transport parallel to heterointerfaces. However, the vertical transport and its understanding in this heterostructure system are nascent. Heterojunction bipolar transistors have fundamental problems having to do with low base p-doping in terms of bipolar transistor standards and inferior emitter quality because of the poor quality Mg doped underlying base layer. The PnP variety is even worse. In terms of unipolar vertical transport structures, double barrier resonant tunneling structures have been reported. However, a closer investigation uncovered fundamental problems with reports in that the negative differential resistance so observed was found to be time dependent and number of sweeps. If the observed phenomenon were to be due to resonant enhanced tunneling none of the above should be associated with it, except some hysteresis.

Recognizing that the reports heretofore have their genesis in traps, we worked to improve the quality by incorporating defect reducing in situ $SiN_x$ mask mediated epitaxial lateral overgrowth and also fine tuning the growth conditions to achieve improved heterointerfaces. Furthermore, simple band edge modeling was performed to search for doping profiles that would lead to electrically nearly symmetrical structures considering the polarization induced charge. By incorporating all of the above, we now observe resonant increase in current at as many as three quantum states of the well, consistent with calculations, albeit at temperatures below 40 K. The remaining problem is that there is still anomalous background current associated with each of the quantum states. Therefore, the quality must be improved further to reduce if not totally eliminate the excess current. Preliminary structures doped with In indicate much better heterostructures in terms of smoothness. Furthermore, DLTS and other investigations we conducted indicate that In doped samples are electronically better as well.

In short, In doping will be used as well as incorporating all that we learned in structures grown on GaN substrates which we believe will give way to tunneling dominated current at resonant states. Once we achieve negative differential resistance at room temperature, we will fabricate structures for Prof. K. Renk for him to test in THz cavities for oscillations. In what follows we detail our investigation up to present in order to give a flavor of the enormous progress made in the last few months.

## 2. Literature review

In addition to the heterojunction field effect transistors and commercialized light emitting diodes in the visible and UV regions, nitride based resonant tunneling diodes and intersubband transition based emitters and detectors are expected to have advantages over GaAs material varieties such as high power capability owing to the larger conduction band discontinuities which should make possible enhanced performance at room temperature.

Although a negative differential resistance (NDR) in nitrides was first reported in 2002 by *Kikuchi et al.,*[1] with a peak-to-valley-current ratio of 32 having been claimed, the mechanism of the observed NDR has been under debate.[2] Current instabilities in AlN/GaN double barrier structures were also observed which have been attributed to either the resonant tunneling processes or charging processes of defects.[3,4] Few other groups[1,5,6] also have joined chorus and claimed observation of NDR presumably due to tunneling related in the nitride system None of them has so far demonstrated high frequency oscillations of any kind. We have argued for a quite a while that NDR observed in must have been due to defects. In fact our earlier results have been consistent with defect mitigated processes although in our case we could maintain NDR for many scans as opposed to one in earlier reports.

*In this report, we will first delve into the simulations which would serve to set the stage as to what can be expected. This will then be followed by our experimental observations and interpretation. We believe that we now are observing increased resonant transmission in our double barrier, single well, structures. However, additional research toward improving the quality of the layers is needed to eliminate the excess current present. Despite the tremendous advances we made recently, we still have a good deal of technological development to reduce if not totally eliminate the excess current. We think that In doping followed by growth on native GaN templates would get us there. In fact In doping has improved the interfacial quality as judged from the number and sharpness of satellite peaks in test superlattice structures we have prepared.*

## 3. Simulations

There have been quite a few reports regarding simulations to achieve oscillations from various forms of GaN based heterostructures/superlattices already.[7,8,9,10,11] We should,

however, mention that the simulation conducted up to recent times assumed the polarization charge was somehow screened by free electrons arriving from some contact with no attention paid to the realistic structures. In our work, we actually had to tweak the doping levels, particularly in the top GaN layer which supplies the carriers, to obtain electrically nearly symmetric structure. In the treatment that immediately follows no concern was paid to the screening issue. However, in the discussion of experimental results, we will introduce the polarization charge and needed carriers for screening that charge.

In an AlGaN/GaN superlattice (SL), to obtain the miniband in SL, *Litvinov* (Waveband) *et al.*[12,13] simulated the band diagram shown in Figure 1, with the consideration of polarization field, but with the assumption that free electrons would come from somewhere such as an infinite source in GaN on top of the last barrier toward the surface. This will be modified to represent real structures that have been realized in our laboratory. During their calculation, 1 eV bowing was used to get the bandgap of AlGaN, and the conduction band offset is given by:

$$\Delta E_c(x) = E_g(x) - E_g^{GaN} - \Delta E_v(x) \approx 0.603x + 0.99x^2 \text{ [eV]}$$

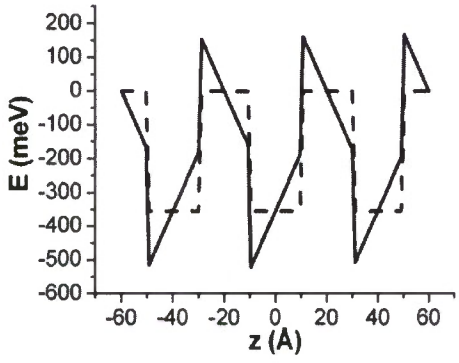


**Figure 1** Conduction band profile in AlGaN/GaN SL (eV) in the direction of growth (angstrom): solid line includes polarization fields; dashed line corresponds to flat-band approximation; x=0.18, $d_b$=$d_w$=20 Å. [Ref. 13]

Numerical calculations[14] with the help of the Poisson-Schrödinger solver[14] confirmed the conduction band offsets calculated using the first-principle valence band offse ts between binary alloys.[15] In solver based calculations the polarization charge is modeled as delta-doped regions at the interfaces. Simulations showed that when Al

composition (x) and SL periods (d) are in the range of 0.18<x< 0.4 and d<50 Å, respectively, the miniband energy dispersion required more than the first nearest neighbor term in the dispersion law in which case the simple cosine-law was normally used in the kinetic equation to study the electron dynamics in a narrow band.

As the result of the simulation optimum, the Al content (x), superlattice period (d), and the parameters of the external circuit were determined and a representative equivalent circuit defined. In the optimized structure, the AlGaN/GaN SL contains 50 pairs, with $d_b$= 9Å and $d_w$ = 15Å barrier and well widths, respectively, and Al%=42%. Complete screening of the polarization fields (flat-band SL) leads to a 10% decrease in the miniband width (low-field mobility). That slow change allows neglecting the carrier concentration dependence of the SL parameters. Both sides of the sample are straddled by highly n-type doped ($10^{19}$ $cm^{-3}$) 0.01 μm-thick layers to provide good ohmic contact. Additional p-doped layer ($p = 1.5\times10^{17}$ $cm^{-3}$ in Figure 2) prevents spillover of electrons from the metal contact. The lattice temperature is assumed to be 300 K. The spatial electron density and evolution of the electrical domains in a 4.7 V biased SL is shown in Figure 2.

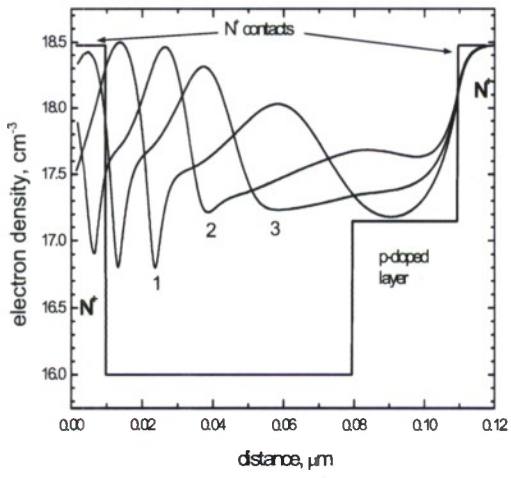


**Figure 2** Spatial distribution of the electron (solid) and doping (dashed) concentration at consecutive times:1-3T/8, 2 – T/2, 3-3T/4, 4-7T/8, where T is the period of oscillations. Courtesy of Dr. V. Litvinov.

To start the oscillations the bias was increased from zero to a value higher than $2LF_{crit}$, where $L$ is the total SL thickness and $F_{crit}$=100 kV/cm for x=0.42 Al. Usually, higher mobility results in higher frequency of oscillations. However, considering that a high current through the structure could damage the ohmic contacts, the practical simulations

were kept at an average current near 100 kA/cm$^2$, which is shown in Figure 3.

Output power $P_f$ and intrinsic efficiency $\eta$ were also calculated based on the simulation results with harmonic oscillations at 200 GHz.[16] For a typical mesa area of 100 μm$^2$, the output power is about 12.5 mW with a (3-6) % intrinsic efficiency.

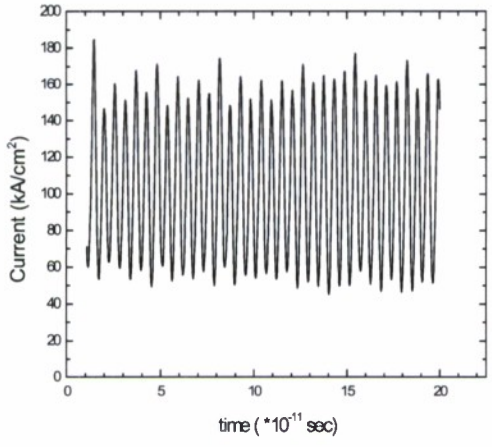


**Figure 3** Current oscillations. [Ref. 16]

## 4. Available experimental data prior to our latest effort

Given the lack of successful history of GaN based superlattices and various complications arising from polarization, double barrier resonant tunneling diodes (RTDs) were chosen to determine the imperative particulars such as composition, thicknesses and doping levels of various layers involved in the RTD stack. Early investigations conducted in our laboratory after some optimization of GaN/AlN based heterojunctions showed negative differential resistance (NDR). As already alluded to earlier, further investigations in our laboratory raised questions about the origin of the NDR observed and we took the default position that the observed NDR is related to defects in the material, a position soundly based on history dependent nature of NDR and its disappearance after a scan in many cases.

In our case, as in previously reported cases, the material quality had to be improved

considerably to avoid excessive leakage to the point where NDR, even of defect origin, could be observed.

For vertical carrier transport, IV characteristics are very sensitive to the dislocations and traps, much more so that the devices relying on lateral carrier transport. RTD and superlattice structures have both been studied experimentally, and the typical DC IV measured at 10K in a 10 pair AlN/GaN SL.[17] The sample was cooled down to 10 K in the dark. Then the IV was measured in again dark, and no NDR was observed (dotted line in the Figure 4). After shining light from a Xe lamp onto the sample, immediately, the NDR appeared under reverse bias but with the peak to valley ratio depending on the sweeping direction. The main difference of this particular sample from the RTD structures, in which NDR was only observed during voltage sweep-up,[18,19] is that the NDR features are more pronounced during sweep-down. Moreover, the NDR features are reproducible no matter how many scans are performed. For a comparison, in the GaN/AlGaN double-barrier RTD grown on a single crystal GaN substrate, the NDR disappeared after several scans, and was partially contributed by electron traps.[18]

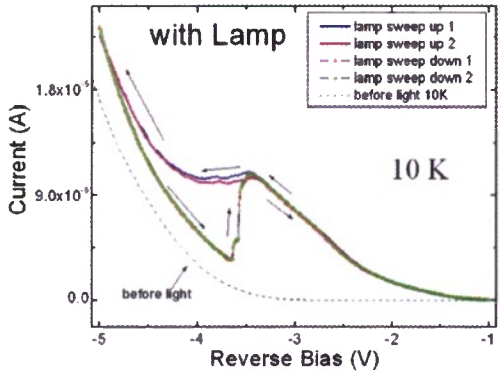


**Figure 4** Reverse bias I-V of 10 pair AlN/GaN superlattice at 10 K with a Xe lamp. [Ref. 17]

## 5. Experimental data of our recent effort

As in our earlier effort, owing to smoother interfaces obtainable, we chose to focus on GaN/AlN RTD structures in the current effort although a low level activity considering the AlGaN barriers is ongoing. Furthermore, structures which are symmetric in terms of

doping levels and also compositional gradient were initially used with no attention paid to polarization induced charge where that charge would come from. However, consideration of that charge and where it would come from lead to what would have been the obvious conclusion that the GaN layer above the top AlN would supply that charge and as a result would be depleted. Consequently, the structure would be asymmetrical in terms of the bandage and also the IV characteristics as will soon be chronicled. This realization led to consideration of doping that the particular GaN layer heavily in an effort to reduce the depletion depth, which is also discussed in this report as "symmetric structure". Further improvement toward the realization of symmetric structure can be obtained by using δ doping. For this to really be effective sheet densities on the order of mid $10^{13}$ $cm^{-2}$ are required. This constitutes nearly one half of a monolayer experiments for which are in progress. However, data for $10^{12}$ $cm^{-2}$ sheet density in addition to high bulk doping have been conducted and are covered here.

### 5.1. Asymmetric Structures

The structural details of the RTD structure are shown in Figure 5(a). The down side of AlN barriers as compared to AlGaN barriers is that the compositional grading and strain-induced polarization is large and cause a large depletion region above the top barrier as illustrated in the energy band diagram of Figure 5(b). The large depletion charge causes large band bending in the same layer. While at the same time the polarization induced charge calls for electron accumulation at the bottom GaN surface just below the bottom AlN barrier (to the right in the figure), The electrons for the accumulation layer come from the top GaN where the depletion occurred. Consequently, the structure is highly asymmetric in terms of the band structure and thus a large asymmetry in the current-voltage characteristic would ensue. In fact, the voltages needed for resonant conditions are so high that the current observed is dominated by excess current with no observation of resonant processes that may take place. As will be discussed shortly, the asymmetry problems were addressed by heavily doping the top GaN which also included δ doping.

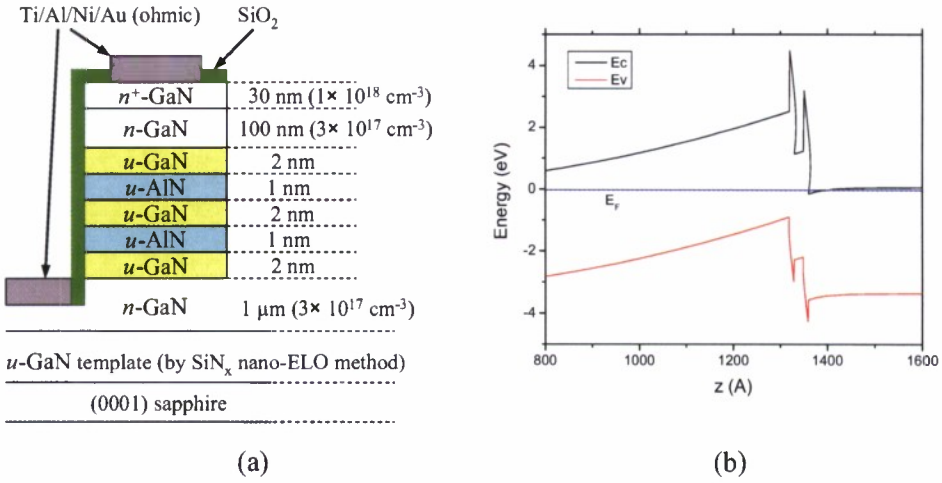


**Figure 5** (a) Schematic diagram of RTD structures with varying well and barrier widths. (b) Energy band diagram obtained from self-consistent solution of the Schrödinger's equation for an RTD structure with 1 nm AlN barriers and 2 nm GaN well (Ga-polarity surface is to the left in the diagram).

The band diagram of the structure shown in Figure 5(a) but under Ga-polarity surface side negatively and positively biased conditions is shown in Figure 6. That shown in Figure 5(b) is for the equilibrium case with no bias. It is clear that when the surface is negatively biased with respect to the bulk in this Ga-polarity sample, tunneling is practically impossible due to the large depletion layer in GaN above the top AlN barrier. However, tunneling should be possible when the bias is positive with respect to the bulk. Unfortunately, the experimental data we obtained in several samples did not indicate any tunneling. We attribute this to excess current being dominant.

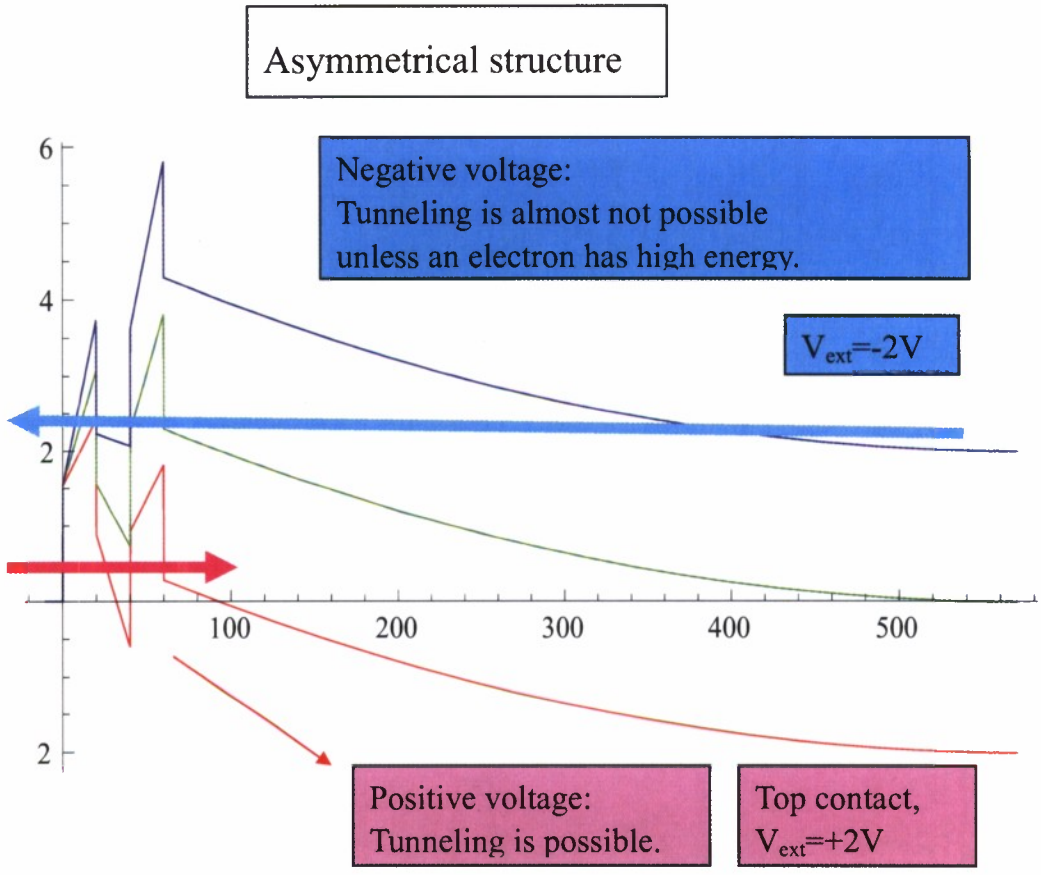


**Figure 6** Band structure of the asymmetric device, with Ga-polarity and top face on the right hand side, under forward and reverse bias conditions. It is clear that tunneling is practically impossible when the top surface is negatively biased, but it is possible when the top surface is positively biased. Courtesy of Dr. V. Litvinov.

RTD structures used in our experiments were grown on GaN templates prepared by MOCVD using *in situ* $SiN_x$ nanonetwork, The role of the nanonetwork is to reduce the extended and thus point defect concentration. For template preparation an AlN nucleation layer was grown on *c*-sapphire, followed by ~ 1 μm-thick GaN, on which $SiN_x$ nanonetwork layers were deposited. A 3 μm-thick undoped GaN layer was then grown by nano epitaxial lateral overgrowth (nano-ELO). As shown in Figure 5(a) these early varieties of RTD structures consist of undoped AlN/GaN/AlN double barriers with 2 nm-thick undoped GaN layers and *n*-GaN on each side.

In order to find the optimum structure, 3 samples with 2 nm GaN wells and Al barriers

of varying thickness (1, 2, and 3 nm) and a sample with 1nm GaN well and 2 nm AlN barrier were grown. The parameters for other layers are shown in Figure 5(a). For device fabrication, 125 μm diameter circular mesa structures were defined by reactive ion etching (RIE). Ohmic contacts were formed by rapid thermal annealing of Ti/Al/Ni/Au (30/100/30/30 nm) at 850 °C for 60s. Additional Ti/Au (30/100 nm) layers were deposited on ohmic contacts for wire bonding. E-beam evaporated 300 nm-thick $SiO_2$ was used for surface passivation. Top contact was biased and bottom contact was grounded during I-V measurements.

As mentioned above, due to the polarization charge, an asymmetry in the IV characteristic should be observed. Figure 7 shows I-V characteristics of RTDs with different structures at room temperature. For 2 nm GaN well thickness, the barrier thicknesses explored are 1, 2, and 3 nm. Furthermore, for a barrier thickness of 2 nm, another sample in which the well width is reduced to 1nm was also prepared in order to raise the quantum states in the well. Regardless of the structure investigated, a rectifying behavior is clearly observed, which arises from the asymmetry of the energy band diagram of the RTD structure due to polarization. The exact nature of current flow can be investigated in order to gain insight, but at this stage it is outside of the scope and goal of this program which is to eliminate it. Given the scarcity of time and funding, our effort would be better spent by focusing on methodology such as growth on GaN substrates which are planned. However, the access current is most likely associated with defect mitigated current at low voltages and in addition thermionic emission current at higher forward voltages. Without delving into it in detail, however, we undertook temperature dependent measurements in order to gain a first order, cursory, insight into the current conduction mechanism.

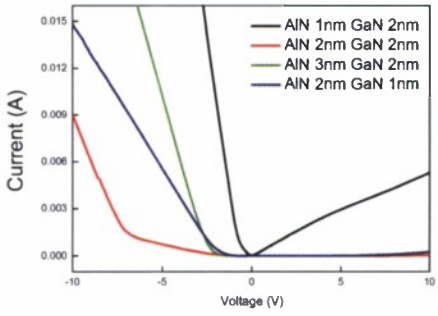


**Figure 7** Room temperature I-V characteristics of RTDs with different barrier and well widths. The electron concentration in n-GaN layer above top AlN barrier is ~ $3x10^{17}$ $cm^{-3}$.

Figure 8 shows temperature dependent I-V characteristics of RTD structures with 1 nm AlN barriers and a 2 nm GaN well. There is a very small change in current with temperature, which indicates that the current conduction mechanism is related to some sort of tunneling process. At first it might appear as if the thin 1 nm AlN layers make carriers tunnel easily through the entire structure involving barriers, the well, and the depletion region even under nonresonant conditions. However, calculation of the transmission probability indicates; see Figure 9, that there are 3 resonant quantum states, which are absent in experimental characteristics of Figure 8, and that the transmission coefficient is increased as compared to the thicker barriers. This means that extrinsic effects such as distributed defect assisted tunneling, which is to a large extent temperature insensitive smeared out the resonant states. In short, this implies the tunneling like current conduction observed is most likely due to defect mitigated tunneling.

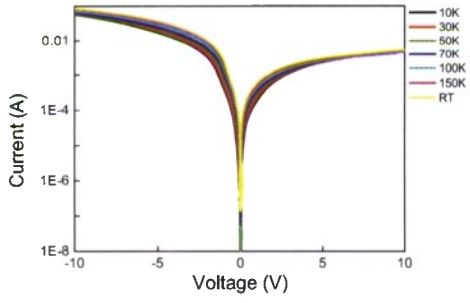


**Figure 8** Temperature dependent I-V characteristics of an RTD structure with 1 nm AlN barriers and 2 nm GaN QW. The energy band diagram is shown in Figure 5(b).

Tunneling probability (transmission coefficient) for a double barrier structure with 2 nm quantum well and for varying barrier thicknesses of 1, 2, and 3 nm with rectangular barriers (meaning no polarization charge, no depletion region and no applied bias) is shown in Figure 9. These calculations were independently conducted by Dr. V. Litvinov and the results agree with our calculations which are shown in Figure 9.

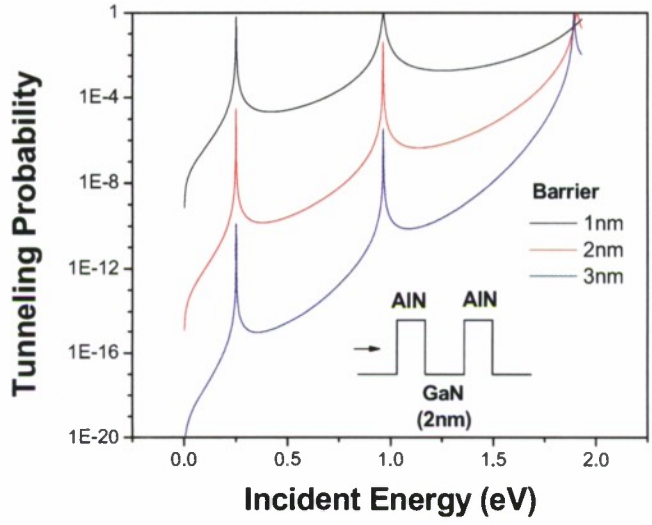


**Figure 9** Tunneling probability (transmission coefficient) for a double barrier structure with 2 nm quantum well and for varying barrier thicknesses of 1, 2, and 3 nm.

When the barrier thickness is increased to 2 nm, the transmission probability vs. energy indicates again 3 resonant levels as shown in Figure 9. On the experimental front, however, a more complicated current conduction mechanism occurs. Figure 10(a) shows temperature dependent I-V characteristics of the RTD structure with 2 nm AlN barriers and a 2 nm GaN well. For small applied voltages (-1 V<V<1 V) and higher temperatures (T>150 K), log(I/V) characteristic has a linear dependence on $V^{1/2}$, where I is the current and V is the applied voltage. This is a characteristic of Pool-Frenkel (P-F) current mechanism. An activation energy of 90 meV is obtained from the IV curves above 150 K. Furthermore, the voltage range at which the P-F occurs is similar to that reported elsewhere for InGaN/GaN light emitting diodes.[20] It has been suggested that such type of current conduction is dominated by a shunt channel with conductivity higher than that of the intrinsic heterojunction.

The resulting shunt currents, interpreted as leakage through screw type dislocations and/or damaged mesa sidewalls, are probably governed by hopping between the nearest neighbor localized electronic states having an activation energy of 90 meV. The genesis of the localized states, beyond screw dislocation, has been suggested as being due to the

dry etching processes and/or post-oxidation during fabrication.[20] This point is still in investigative state in our laboratory as the devices so reported here were fabricated by reactive ion etching formed mesas. We recently added an inductively couple plasma etching system which by virtue of much higher plasma density can function with much lower power levels and thus lower ion energies which are harmful to the material being fabricated.

In a range of applied voltages (-5.4 V<V<-2.2 V) another P-F mechanism appears to begin to dominate the current conduction, which is shown in Figure 10(c) and (d). In this region, the applied bias voltage seems to be larger than the internal voltage needed for flat band ($V_{bi}$) conditions. This means that the current is limited by the series resistance. Therefore, the applied effective voltage for the P-F is $V-V_{bi}$ because $V_{bi}$ (~ 1.2 V) is needed to reach the flat band conditions. According to reference 20, in the low applied voltage range the dominant current may be the leakage current. At medium biases, above the voltage range, the current will be limited by junction (double barrier + depletion region) resistance. The resistance in the depletion region may be larger than that in the double barrier region. In other words, in order for electrons to flow from the top contact to the bottom contact mainly unimpeded, the conduction band should be flat. Otherwise the carriers have to tunnel through the depletion region which is unlikely and thus causes the current level very low. So for flattening band in depletion region, some voltage is needed. 1.2 V comes from best one among several trials to fit I-V to F-P formula. As shown in Figure 10(c), $\log(I/(V-V_{bi}))$ has a linear dependence on $(V-V_{bi})^{1/2}$. The effective barrier height plotted in this region as a function of $(V-V_{bi})$ in Figure 10(d) gives 33 meV at $V=V_{bi}$. This is likely to be associated with shallow donor like defects as this energy is very close to the Si donor energy level (30 meV) in GaN. Therefore, the P-F mechanism dominant in the voltage range of -5.4 V<V<-2.2 V may be caused by shallow donor like defects. It should also be noted that 1.2 V for $V_{bi}$ is smaller than expected, which indicates that there is some barrier lowering phenomena taking place such as that which can be caused by defects. This argument follows the strategy used in reference 20. The only difference is that the current source in reference 20 is holes while the current is due to electrons in our case. The activation energy reported in reference 20 which is 190 meV is very close to the ionization energy of magnesium.

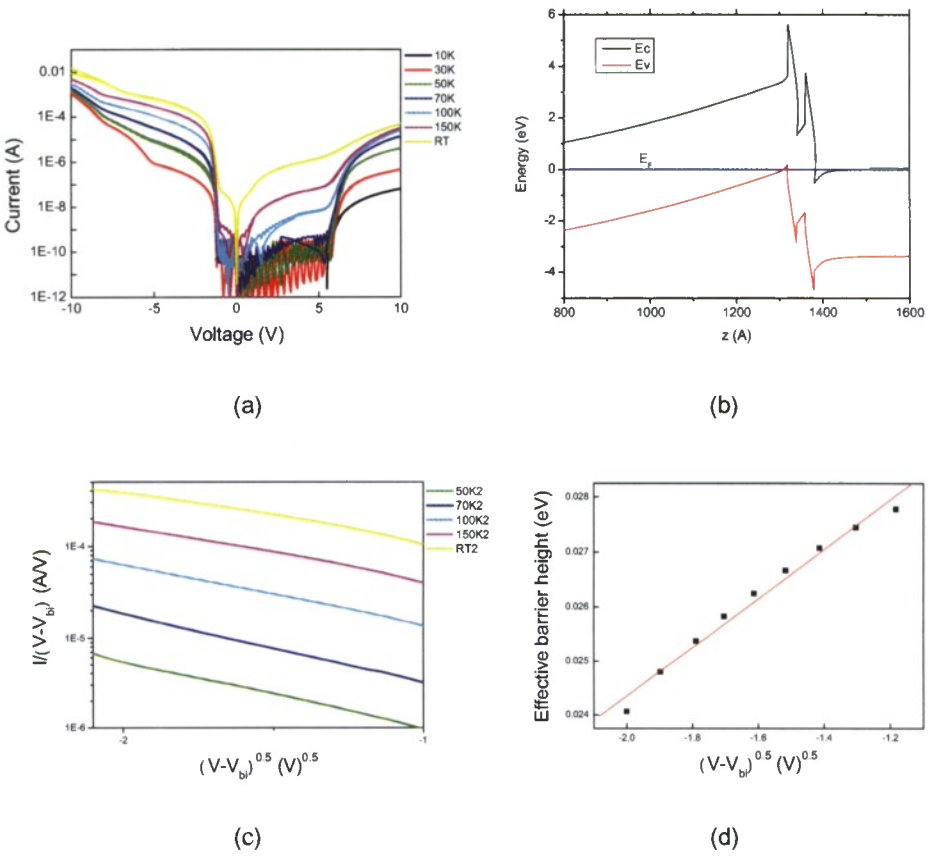


**Figure 10** (a) Temperature dependent I-V characteristics and (b) energy band diagram of an RTD structure with 2 nm AlN barriers and a 2 nm GaN well. Plots of (c) $(I/(V-V_{bi}))$ vs. $(V-V_{bi})^{1/2}$ at various temperatures, and (d) effective barrier height in P-F for bias voltage. The solid line in (d) is a linear fit to the data.

For RTD structures having even thicker AlN barriers (3 nm), applied voltage required to achieve flat bands is higher. As shown in Figure 9 the tunneling probability is drastically reduced compared to the 2 nm and 1 nm barrier cases. Still there are 3 resonant states. If other current conduction routes were to be eliminated, by growth of much higher quality samples and appropriate design of the structure, for example, tunneling current through the resonant states might be observed. Figure 11(a) shows temperature dependent I-V characteristics of an RTD structure with 3 nm AlN barriers. The P-F mechanism is seen to dominate in the very low voltage range as in relatively thinner barrier RTDs. As shown in Figure 11(c), log (I) depends linearly on V in the

range -1.3 V<V<-0.8 V, and the ideality factor is larger than 4, which indicates that this current is neither due to simple diffusion (ideality factor is 1) nor generation-recombination (ideality factor is 2). In the same applied voltage range a very low activation energy of the order of 1 meV was measured. Figure 11(d) shows a linear relation between log ($I/V^2$) and $V^{-1}$ in the same range at low temperature (T<150 K), which is characteristic of tunneling. Except for the applied voltage range of -0.8 V<V<2 V, the activation energy is very small. As the voltage is swept, a hysteresis is observed for V>3 V, suggesting that the current mechanism is tunneling related to localized states. Figure 11(a) clearly shows that the current mechanism in the range of 1 V<V<2 V changes from P-F to tunneling.

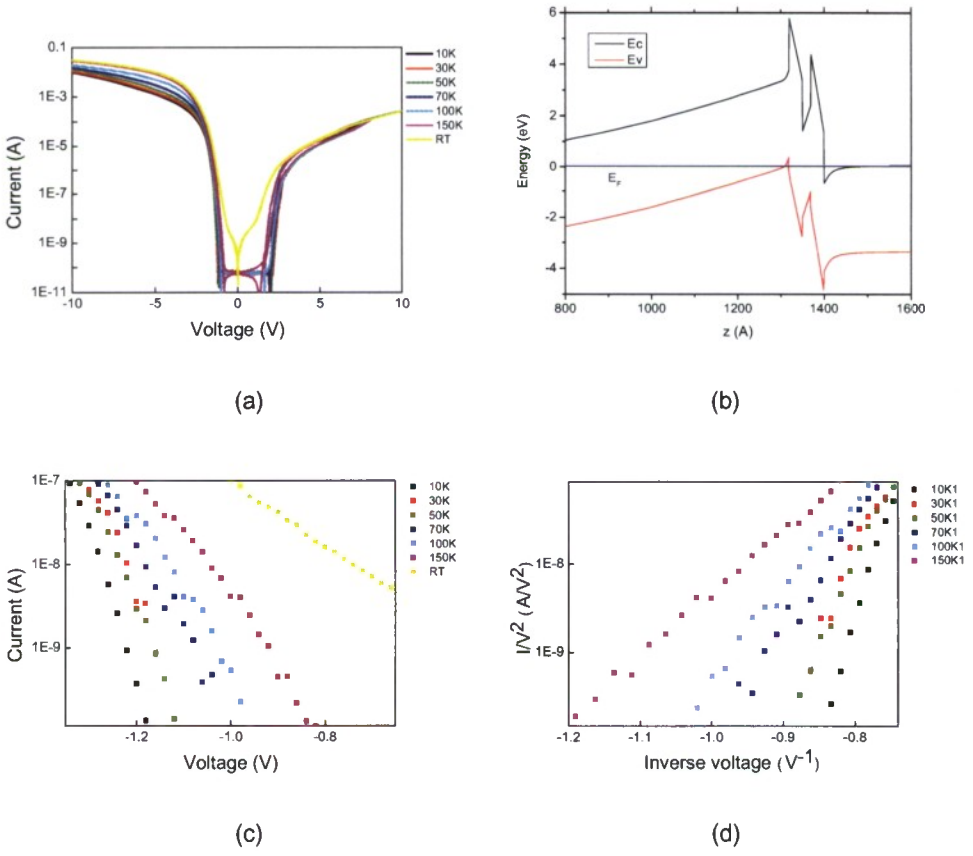


**Figure 11** (a) Temperature dependent I-V characteristics and (b) energy band diagram of an RTD structure with 3 nm AlN barriers and 2 nm GaN well and. Plots of (b) I vs. V in semilog scale for -1.3<V<-0.7 V and (c) ($I/V^2$) vs. $V^{-1}$ at temperatures below T<150 K.

We also investigated RTD structures with narrower wells allowing more confinement. Figure 12 shows the temperature dependent I-V characteristics of an RTD structure with 2 nm AlN barriers and 1 nm GaN QW. The transmission probability for this well width for 1, 2, and 3 nm AlN barrier thickness are shown in Figure 13 which clearly demonstrate that there is only 1 resonant state due to large confinement. In terms of the experimental data, for negative applied voltages the behavior is similar to that of RTDs with 2nm AlN barriers and 2nm GaN well. However, for positive bias voltages the current voltage characteristics are similar to those of RTDs with 3nm AlN barriers in which defect related tunneling current was dominant.

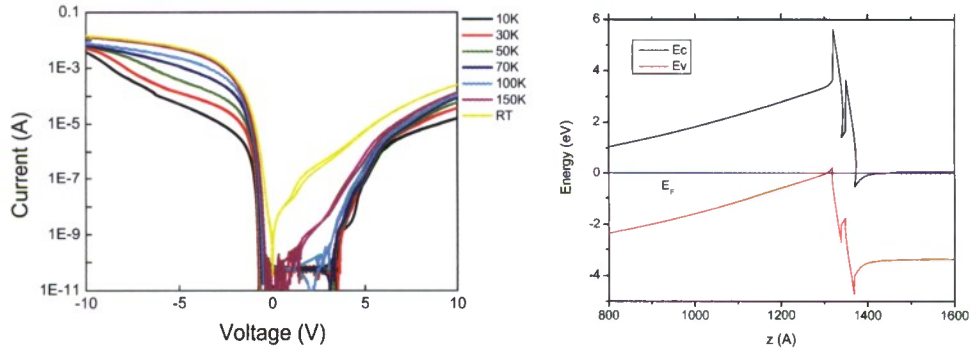


(a) (b)

**Figure 12** (a) Temperature dependent I-V characteristics and (b) energy band diagram of an RTD structure with 2 nm AlN barriers and 1 nm GaN well.

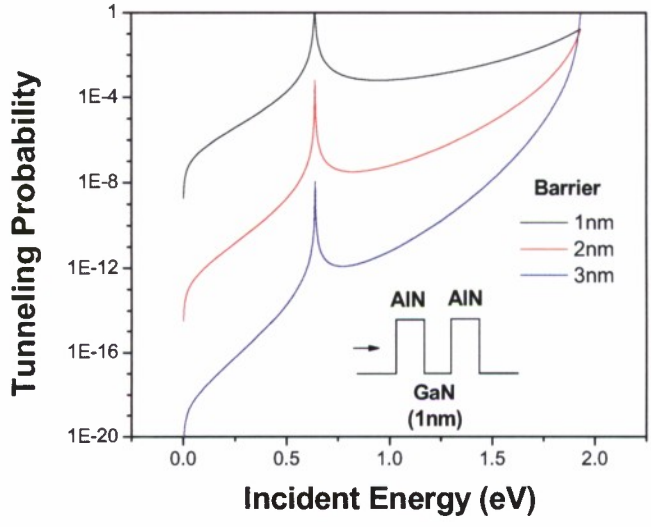


**Figure 13** Tunneling probability (transmission coefficient) for a double barrier structure with 1 nm quantum well and for varying barrier thicknesses of 1, 2, and 3 nm.

In short, from the analysis of RTD structures with varying barrier widths one might at first conclude that 1 nm barriers are too thin, resulting in tunneling even at very small biases. However, calculations of the tunneling probability indicate, see Figure 13, that although there is one resonant state, everything else being correctly done one might be able to observe the tunneling state. The current conduction in RTDs with 3 nm are dominated by trap-assisted tunneling over most of the applied voltage range due to defects originating from possibly increased strain in the GaN well due to thicker AlN barriers and even reduced quality AlN due to partial relaxation. RTD with 2 nm AlN barriers and 1 nm GaN well shows P-F is the main current conduction mechanism. In spite of the use of $SiN_x$ nanonetwork ELO templates for reduction of defects, the layer quality remains in need of further improvement, e.g. by growth using In doping and on bulk GaN templates, both of which are in process, to observe the real negative differential resistance in RTDs. It should also be mentioned that in parallel to technology development, optimization of the band bending is also required as asymmetric I-V characteristics were observed in all the structures due to the wide depletion regions above the top AlN barrier. In what follows below, we switch gears and begin to discuss the structures where the GaN layer atop the top AlN barrier is doped

very heavily in an effort to reduce the depletion region.

### 5.2. Structures with increased doping above the top AlN barrier

We mentioned the depletion depth on top of the top barrier as being too large and causing sizeable asymmetry in the structures. The depletion region width in question can be reduced by increasing doping in the n-GaN layer above the top AlN barrier. To circumvent this impediment and investigate the impact, we incorporated either a heavily doped GaN layer with $5x10^{18}$ $cm^{-3}$ carrier concentration and in some cases a delta doped layer. Figure 14 shows the RTD sample structure with the heavily doped n-GaN layer and the calculated conduction band edge diagram for a series of doping levels, namely $10^{17}$ $cm^{-3}$, $10^{18}$ $cm^{-3}$, and 5x $10^{18}$ $cm^{-3}$ together with δ doping in the amount of $10^{12}$ $cm^{-2}$. As expected, the calculations indicate the depletion region in GaN above the top AlN barrier has been reduced significantly to below 20 nm, but still larger than desired. The delta doping approach helps reduce the thickness theoretically down to negligible levels.

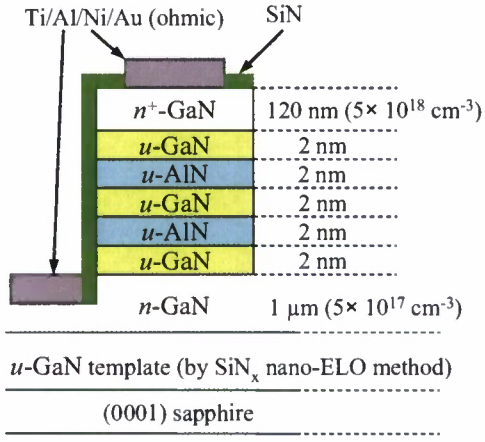


(a)

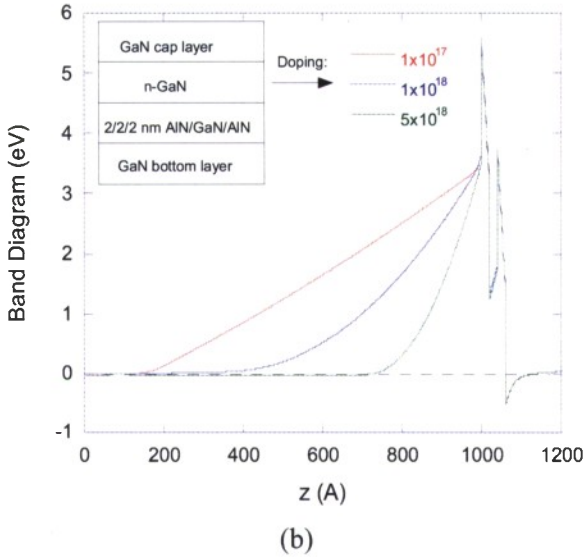


**Figure 14** (a) Schematic diagram and (b) Conduction band edge diagram of the RTD structure with the GaN layer above the top AlN barrier doped at $1x10^{17}$ $cm^{-3}$, $1x10^{18}$ $cm^{-3}$, and $5x10^{18}$ $cm^{-3}$. Note that we used $5x10^{18}$ $cm^{-3}$ in our experiments to reduce the depletion layer width as much as possible.

Let us first discuss the calculated IV characteristics to set the framework as to what can be expected. In order to reduce the complexity of calculations to the point of being manageable without expansive codes, we assumed rectangular barriers with no polarization charge and no depletion region. Doing the calculations for 1, 2, and 3 nm barriers with 2 nm well, the tunneling probability vs. the electron energy resulted in the data shown in Figure 9.

Figure 15 (a) and (b) show respectively the temperature dependent I-V characteristics for a device having a highly doped top GaN ( $5x\ 10^{18}$ $cm^{-3}$) and additional delta doping of $10^{12}$ $cm^{-2}$ (which we now know is too small and needs to be increased which is in progress) with 2 nm barriers and 2 nm quantum well. The I-V data for all temperatures are almost fully symmetric, with the forward current as large as the reverse current unlike the case for the samples discussed above which lacked the highly doped layer above the top barrier. This symmetry is ascribed to the substantially reduced depletion region above the top barrier. Additionally, the I-V data show close to linear behavior and very weak temperature dependence for temperatures above 150 K. At low temperatures, especially at 10K, at least three different conduction channels are clearly observed.

Sudden increases in current represent start (or end of reverse sweep) of the conduction through an additional channel above certain thresholds. We believe that these channels are associated with the 3 resonant quantum states in the well as shown in the transmission probability calculations of Figure 9. For the data at 10 K, the sudden jump in the current at ~ ± 1.15 V occurs without any noticeable hysteresis between the positive and negative sweeps. The next jump occurs at ± 3.6 V in the forward sweep and at ± 2.3 V in the reverse sweep. It should be noted that one needs to make sure the lack of hysteresis is not due to the measurement details of the Keithley 4200 parameter analyzer used for measurements which obtains many data points for the same bias condition and gives the average value as the output parameter.

The above mentioned abrupt changes in the current level could be explained by some quantum phenomena related to phase transition at a specific condition or resonant quantized energy level in double barrier structure. Since the phenomenon occurs at multiple voltages, the latter explanation is much more likely and is supported by Figure 9. However, absence of negative differential resistance, if true, suggests a more complicated conduction mechanism. As mentioned the nature of the parameter analyzer must be considered as well as taking the same data with a curve tracer. Complicating factor is that, hysteresis observed for the second current jump at higher applied voltage might suggest contribution from traps and or natural charge accumulation related instabilities observed in RTD structures as exemplified in GaAs based varieties.[21] Recognizing these, we have undertaken additional steps to enhance the materials quality which includes doping with In and growth on native GaN substrates.

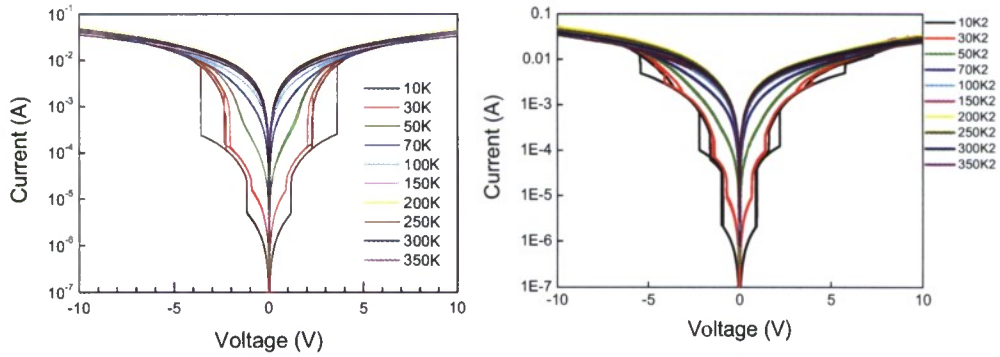


(a) (b)

**Figure 15** Temperature dependent I-V characteristics of RTD structure having 2 nm AlN barriers, a 2 nm GaN well, and a heavily doped ($5x10^{18}$ $cm^{-3}$) n-GaN layer above the top AlN barrier (a) and $5x10^{18}$ $cm^{-3}$ plus $10^{12}$ $cm^{-2}$ delta doping (b).

As mentioned previously and in the case of band structure, the current voltage characteristics are easier to calculate with no depletion region. Calculations which include both of the above can be done with specialized software which are available and can be looked into. However, the calculations with the simplifying assumptions mentioned above are still helpful in our efforts to gain insight and also design device structures. The I-V characteristics calculated so (neglecting the polarization fields and the depletion region) for 2nm barriers and 2 nm well are shown in Figure 16. As in the case of Figure 9 dealing with tunneling properties, the calculated IV is symmetrical although the features are not yet reproduced in experiments.

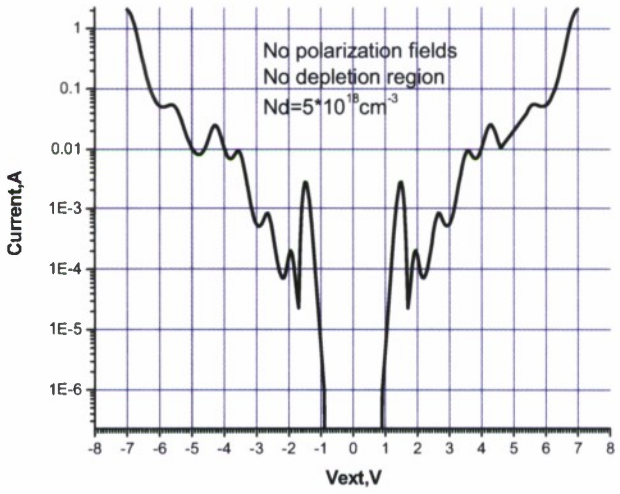


**Figure 16** I-V characteristics calculated for a structure with 2 nm barriers and 2 nm well and Nd=5x10$^{18}$cm$^{-3}$ doping level in the GaN above the top barrier. Neither any depletion region is put in the calculations, nor the effect of the polarization charge is included. Courtesy of Dr. V. Litivinov.

The IV characteristics shown in Figure 16 do not exactly match the transmission probability of Figure 9 dealing with tunneling properties because the shape of the barriers and thus the transmission coefficient change with the applied bias and polarization. If we progressively enhance the strength of the simulations and include the effect of applied bias but continued to neglect the effect of polarization charge, the resulting band structure and transmission probabilities for applied biases of 0, 1 and 2 V are shown in

Figure 17.

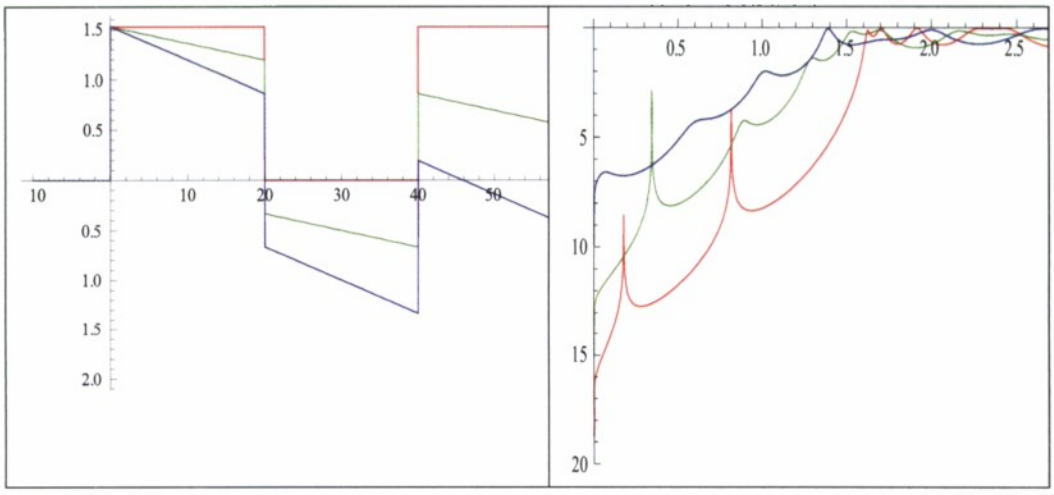


**Figure 17** The band structure (left) and the transmission probability (right) for a structure with 2 nm barriers and 2 nm well and Nd=$5x10^{18}cm^{-3}$ doping with Red-$V_{ext}$=0, green-$V_{ext}$=1V, blue-$V_{ext}$=2V. Polarization fields and depletion region are not included in the model. Courtesy of Dr. V. Litivinov.

If we now include polarization charge, but no bias and no depletion region the transmission probability changes as shown in Figure 18.

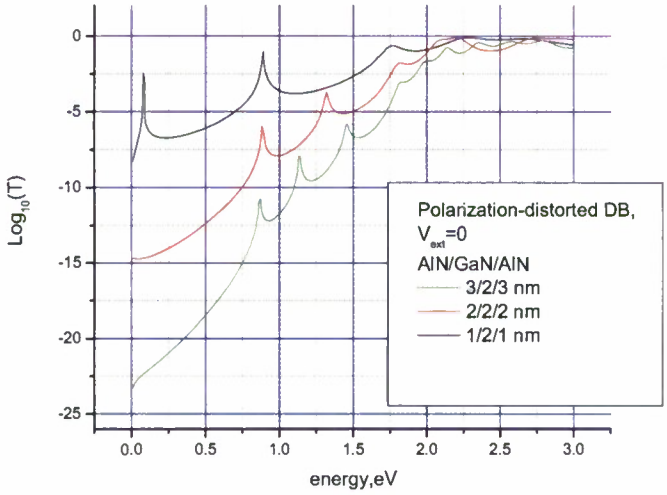


**Figure 18** Tunnel transmission probability for structures with 1, 2, 3 nm barriers and 2 nm well with Polarization-distorted QW structure (no depletion region). The difference between this and that of Figure

9 is the including of polarization charge. Courtesy of Dr. V. Litivinov.

Clearly, calculations which include polarization charge, any depletion and bias are needed which can be done with more sophisticated models which can be obtained if funds are available or collaborations can be established with those who have access to such codes.

### 5.3.Structures with increased doping together with δ doping above the top AlN barrier

In order to reduce the depletion layer width in the GaN above the top AlN barrier, we also incorporated, in addition to $5x10^{18}$ $cm^{-3}$ bulk doping, a δ-doped layer. Figure 19 shows the conduction band edge of an AlN/GaN/AlN (2nm/2/nm/2nm) RTD with no δ-doping, and δ-doping in the amount of $10^{12}$, $10^{13}$, and $5x10^{13}$ $cm^{-2}$ just above the top barrier in addition to $5x10^{18}$ $cm^{-3}$ bulk doping in the GaN layer above the top barrier. Clearly, high δ-doping reduces the depletion depth further. However, in our preliminary experiments, the δ-doping level was chosen to be $10^{12}$ $cm^{-2}$ which means that we will not expect much improvement. Nevertheless for the sake completeness, the data are included.

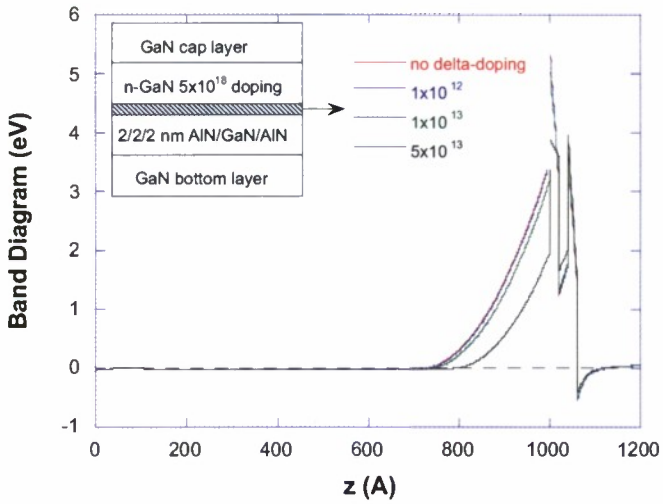


**Figure 19** The conduction band edge diagram of 2nm/2/nm/2nm/ (AlN/GaN/AlN) RTD structure with bulk GaN on either side, but with no δ-doping, and δ-doping in the amount of $10^{12}$, $10^{13}$, and $5x10^{13}$ $cm^{-2}$ just above the top barrier in addition to $5x10^{18}$ $cm^{-3}$ bulk doping in the GaN layer above the top barrier.

Figure 20(a) shows the RTD sample structure with the Si δ-doping layer that is also used to reduce the depletion layer width above the top AlN barrier, and Figure 20(b) shows the temperature dependent I-V characteristics. There is very weak temperature dependence above 100 K. This sample shows similar I-V characteristics to the sample with heavily doped GaN top layer. All current jumps also show hysteretic behavior. To a first sight contribution from traps and or the natural carrier accumulation observed in RTD structures as exemplified in GaAs based varieties[21] might be the genesis. We should note, however, that the I-V curves shown in Figure 15, Figure 20(b) and Figure 21(a) were reproducible for many sweeps both in forward and reverse directions suggesting that current conduction is not dominated by charge trapping and release, and no degradation in device performance was observed. Further measurements using a curve tracer (when voltage swept with 240 Hz) produced similar results with stable I-V characteristics. Figure 20(c) shows a curve tracer image of I-V characteristics near 1.4 V at 10K. Abrupt current jumps and hysteresis are shown to be manifested. The temperature dependent I-V images near 5V are shown in Figure 20(d). The current jump phenomenon disappears with increased temperature above 40 K.

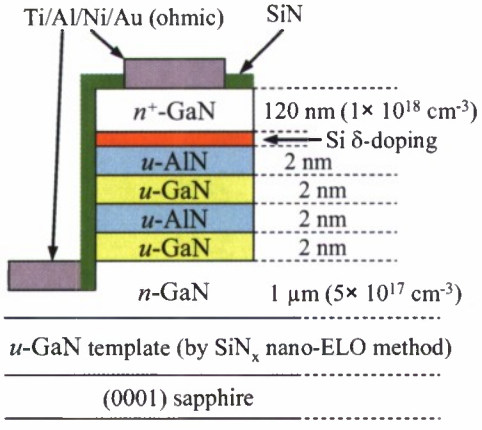


(a)

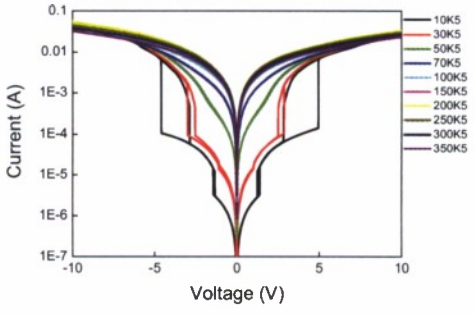


(b)

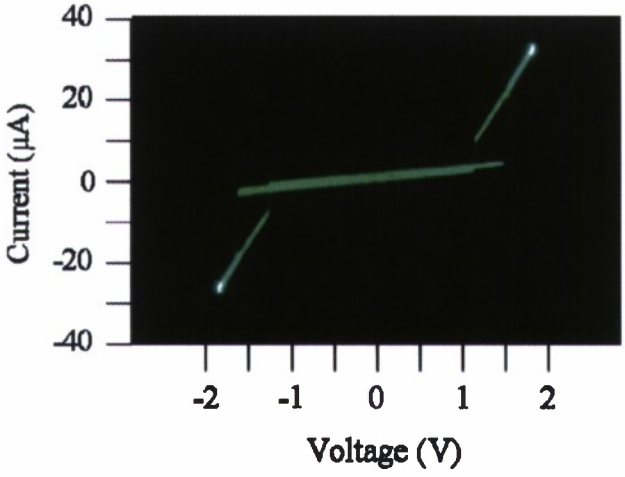


(c)

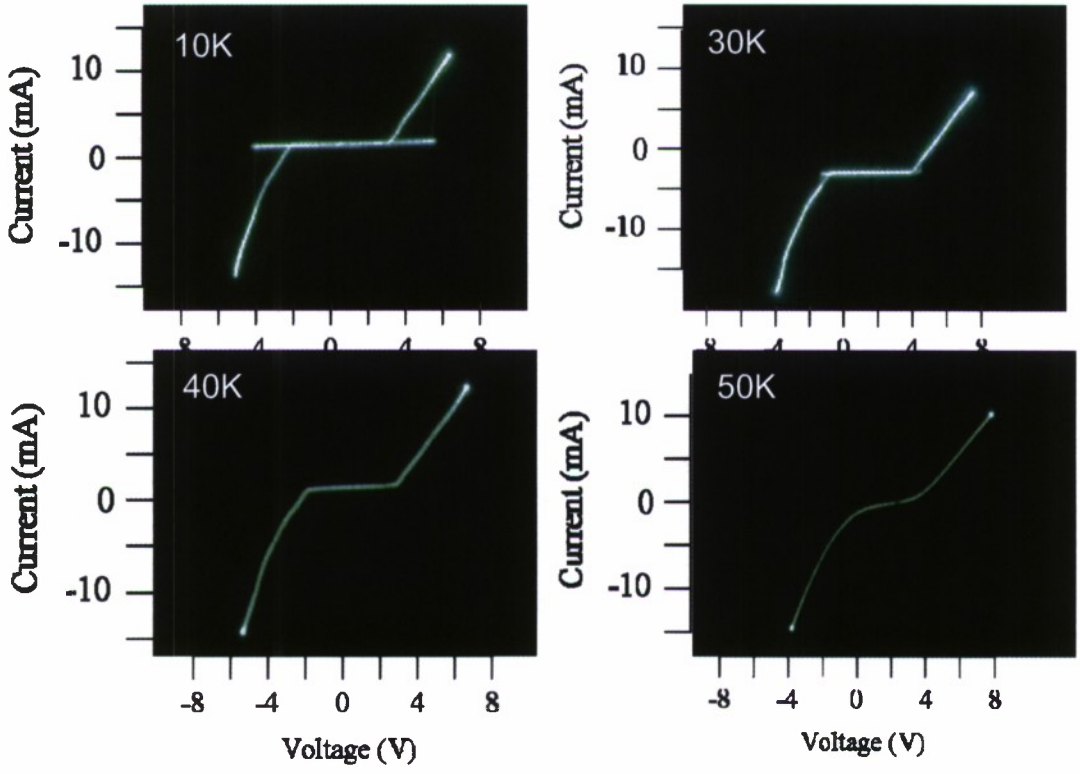


(d)

**Figure 20** (a) Schematic diagram and (b) temperature dependent I-V characteristics of an RTD structure with 2 nm AlN barriers, a 2 nm GaN well, and a Si δ-doping layer above the top AlN barrier. (c) Curve tracer image of I-V characteristics near 1.4 V at 10 K and (d) images of temperature dependent I-V near 5 V.

It is known that the number of defects per device is reduced by reduction of the lateral device area. In cases where the defects are inhomogenously distributed, some devices may even have fewer defects than expected from the average defect density. In order to check the areal size effect on device performance, we investigated small devices (6 μm in diameter). Figure 21(a) shows temperature dependent I-V characteristics of a small RTD device with δ-doping layer in logarithm scale. The small RTD device has relatively small current jump in magnitude compared with the larger ones. And after the current jump, current at higher applied voltage looks unstable. Figure 21(b) shows I-V image from the curve tracer at 10K in which current near 5 V is not stable too. The effect of the sidewall damage on current conduction mechanism is now an issue. There is a possibility that during forming of the mesas using ICP-RIE defects on sidewall were induced by high energy ions which affect the current mechanism in RTD. Since the fabrication of these small area devices, we installed an inductively couple plasma etching system with higher plasma density which allows operation with lower ion energies. In addition to exploring ICP formed sidewalls, we will also investigate any wet chemical etching process to help reduce, if not totally eliminate, the sidewall damage.

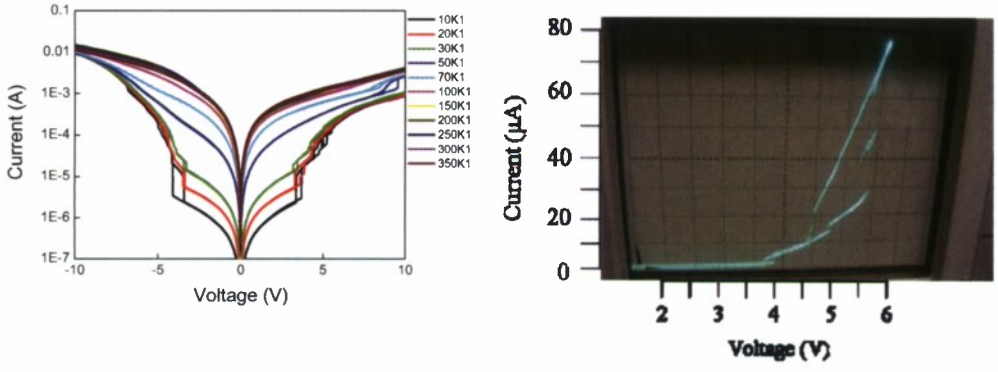


(a) (b)

**Figure 21** (a) Temperature dependent I-V characteristics of a 6 μm diameter RTD structure with δ-doping layer and (b) temperature dependent I-V characteristics near 5 V measured at 10 K with a curve tracer.

## 6. Conclusions

In summary, RTD structures with different barrier and QW thicknesses and doping levels have been investigated in our quest to observe resonant tunneling phenomenon in GaN based system for the first time. We investigated what appear to be symmetrical structures in terms of doping levels. However, due to polarization charge and field induced by it, a depletion layer on top of the upper AlN barrier and an accumulation layer below the bottom AlN barrier are formed. Consequently, the I-V characteristics are asymmetrical and observation of resonant states would occur at high applied biases wherein extrinsic current mechanisms become dominant and obscure any resonant tunneling based current. This is by and large what we observed experimentally which efforts to delineate various current conduction mechanisms. However, when the doping level in the GaN layer above the top AlN barrier is increased and in some cases augmented by a $\delta$ doping to substantially reduce the depletion layer width to allow carrier tunneling through it, the I-V characteristic became symmetrical. What is more exciting is that we believe observed abrupt current jumps for temperatures below 30 K at three different voltages are associated with resonant states. Calculations also suggest the presence of 3 resonant states for the well and barrier dimensions investigated. Stability of the abrupt rise in current regardless of number of positive or negative sweeps support the above conclusions. However, there appears to be excess current associated with each of the three states as well. This implies that while we have improved the layer quality and device design substantially, we have some ways to go yet. This we intend to do with In doping which led to sharper interfaces as judged by satellite peaks in special superlattice structures designed for preliminary characterization. The RTD structures with In doping have been grown and are in the process of being fabricated. When all the optimization schemes are developed, the ultimate structures will be grown on GaN substrates in an effort to reduce the excess current and observe NDR at room temperature and to undertake experiments for THz generation.

References


[1] A. Kikuchi, R. Banai, K. Kishino, C.-M. Lee, and J.-I. Chyi; "AlN/GaN double-barrier resonant tunneling diodes grown by rf-plasma-assisted molecular-beam epitaxy", Appl. Phys. Lett. **81**, 1729 (2002).

[2] A. E. Belyaev, C. T. Foxon, S. V. Novikov, O. Makarovsky, L. Eaves, M. J. Kappers, and C. J. Humphreys; "Comment on "AlN/GaN double-barrier resonant tunneling diodes grown by rf-plasma-assisted molecular-beam epitaxy"; Appl. Phys. Lett. **81**, 1729 (2002)]", Appl. Phys. Lett.; **83**, 3626 (2003).

[3] C. T. Foxon, S. V. Novikov, A. E. Belyaev, L. X. Zhao, O. Makarovsky, D. J. Walker, L. Eaves, R. I. Dykeman, S. V. Danylyuk, S. A. Vitusevich, M. J. Kappers, J. S. Barnard, and C. J. Humphreys; "Current-voltage instabilities in GaN/AlGaN resonant tunnelling structures", Phys. stat. sol. (c) **0**, 2389 (2003).

[4] A.E. Belyaeva, O. Makarovskya, D.J. Walkera, L. Eavesa, C.T. Foxona, S.V. Novikova; L.X. Zhaoa, R.I. Dykemanc, S.V. Danylyukd, S.A. Vitusevichd, M.J. Kapperse, J.S. Barnarde, and C.J. Humphreyse; "Resonance and current instabilities in AlN/GaN resonant tunnelling diodes", Physica E **21**, 752 (2004).

[5] S. N. Grinyaev and A. N. Razzhuvalov; "Resonant electron tunneling in GaN / $Ga_{1-x}Al_xN$ (0001) strained structures with spontaneous polarization and piezoeffect", Phys. Solid State **43**, 549 (2001).

6 S. Golka, C. Pflügl, W. Schrenk, and G. Strasser, C. Skierbiszewski, M. Siekacz, I. Grzegory, and S. Porowski; "Negative differential resistance in dislocation-free GaN/AlGaN double-barrier diodes grown on bulk GaN", Appl. Phys. Lett. **88**, 172106 (2006).

[7] V.I. Litvinov, presented at "Challenges facing ZnO and GaN: Facts and Myths", Oct, 2007 Richmond VA.

[8] I. Gordion, A. Manasson, and V.I. Litvinov "Electrical Domains and Submillimeter Signal Generation in AlGaN/GaN Superlattices"; IEEE Trans. Electr. Devices **53**, 1294 (2006).

[9] V. I. Litvinov, and A. Manasson; "Superlattice in an interminiband resonance ac field", J. Appl. Phys. **98**, 043505 (2005).

[10] V.I. Litvinov, and A. Manasson; "Large-signal negative dynamic conductivity and high-harmonic oscillations in a superlattice", Phys.Rev. B **70**, 195323 (2004).

[11] V.I. Litvinov, A. Manasson, and D. Pavlidis; "Short-period intrinsic Stark GaN/AlGaN superlattice as a Bloch oscillator", Appl. Phys. Lett. **85**, 600 (2004).

[12] V.I. Litvinov, and A. Manasson; "Large-signal negative dynamic conductivity and high-harmonic oscillations in a superlattice", Phys.Rev. B **70**, 195323 (2004).

[13] V.I. Litvinov, A. Manasson, and D. Pavlidis; "Short-period intrinsic Stark GaN/AlGaN superlattice as a Bloch oscillator", Appl. Phys. Lett. **85**, 600 (2004).

[14] Available online at: http://www.nd.edu/~gsnider/

[15] H. Wei and A. Zunger; "Calculated natural band offsets of all II–VI and III–V semiconductors: Chemical trends and the role of cation d orbitals", Appl. Phys. Lett. **72**, 2011, (1998).

[16] V.I. Litvinov, presented at "*Challenges facing ZnO and GaN: Facts and Myths*", Oct. 2007 Richmond, VA.

[17] J.Xie, Ü. Özgür and H. Morkoç, presented at "*Challenges facing ZnO and GaN: Facts and Myths*", Oct. 2007 Richmond VA.

[18] S. Golka, C. Pflügl, W. Schrenk, and G. Strasser, C. Skierbiszewski, M. Siekacz, I. Grzegory, and S. Porowski; "Negative differential resistance in dislocation-free GaN/AlGaN double-barrier diodes grown on bulk GaN", Appl. Phys. Lett. **88**, 172106 (2006)

[19] J. Xie, Ph.D thesis, Chapter Three, Virginia Commonwealth University (2007).

[20] L. Hirsch and A. S. Barrière, "Electrical characterization of InGaN/GaN light emitting diodes grown by molecular beam epitaxy", J. Appl. Phys. **94**, 5014 (2003).

[21] V. J. Goldman and D. C. Tsui; "Observation of intrinsic bistability in resonant-tunneling structures", Phys. Rev. Lett. **58**, 1256 (1987).